MINIMUM SIMPLEX SEMISUPERVISED UNMIXING

Behnood Rasti[⋆†]*, Xander Haijen*[‡]*, Bikram Koirala*[‡]*, Paul Scheunders*[‡]

[⋆] Remote Sensing Laboratory, School of Rural, Surveying and Geoinformatics Engineering,
National Technical University of Athens, Greece
[‡] Imec-VisionLab, Department of Physics, University of Antwerp, Belgium

ABSTRACT

Library-based unmixing is a spectral unmixing strategy that leverages large pre-existing libraries of spectra. Despite its utility, current methods struggle with complex data containing noise or intrinsic material variability. They also lack a robust geometric modeling, which is central to linear mixing models. As a result, existing approaches fail to effectively incorporate the inherent geometry of the data, which is crucial for distinguishing between similar materials. To address these limitations, we propose MiSiSUn (Minimum Simplex Semisupervised Unmixing). MiSiSUn introduces a novel, semi-supervised geometric unmixing framework that integrates the data geometry into the library-based unmixing process using a simplex volume penalty term and an archetypal analysis-based model. Experimental results demonstrate that MiSiSUn significantly outperforms state-of-the-art semi-supervised unmixing methods with performance gains ranging from 1 dB to over 3 dB compared to existing approaches. Furthermore, application to a real dataset shows that MiSiSUn produces visual interpretations that closely align with geological reference maps. MiSiSUn was implemented using PyTorch, which is open-source and available at `https://github.com/BehnoodRasti/MiSiSUn`. Moreover, we provide a dedicated Python package for Semisupervised Unmixing, which is open-source and includes all the methods used in the experiments for the sake of reproducibility

***Index Terms*—** Library-based unmixing, semi-supervised, archetypal analysis, minimal volume constraint

1. INTRODUCTION

Spectral unmixing is an important hyperspectral image analysis technique that aims to decompose mixed pixel spectra – which contain several distinct materials – into constituent material signatures (known as endmembers (EMs)) and their fractional abundances [1, 2]. There are three main strategies for performing unmixing: (1) sequential unmixing (first extracting EMs and then estimating abundances), (2) unsupervised unmixing (simultaneous estimation of EMs and abundances) and (3) library-based semi-supervised unmixing, which uses an overcomplete dictionary of spectral signatures as endmembers. This dictionary is then used to estimate the abundances.

Sequential unmixing often suffers from error propagation, where poor EM estimates due to, e.g., the absence of pure pixels in the image, lead to poor abundance estimates. Similarly, unsupervised unmixing methods often struggle in highly mixed scenarios due to the ill-posed nature of the problem and the non-uniqueness of the solution. Classical library-based unmixing methods require accurate EM libraries that contain exactly the EMs found in the image [3]. However, conditions such as atmospheric effects, noise and intrinsic material variability can lead to a library mismatch, which prevents accurate unmixing. Furthermore, standard sparse unmixing lacks the strong geometric interpretation of other unmixing methods and typically avoids the abundance sum-to-one constraint (ASC) since it conflicts with sparsity penalties.

In this paper, we propose the **Minimum Simplex Semisupervised Unmixing (MiSiSUn)** method, which combines the strong geometric foundations of sequential and unsupervised methods with the advantages of using spectral libraries. Based on Archetypal Analysis, MiSiSUn creates virtual EMs (archetypes) and is highly suitable for unmixing highly mixed scenes. We derive an algorithm based on the Alternating Direction Method of Multipliers (ADMM) framework to solve the resulting nonconvex optimization problem. The resulting algorithm is very suitable for parallelization and can therefore be implemented efficiently on a GPU.

2. RELATED WORKS

2.1. Linear Mixing Model

The traditional low-rank Linear Mixing Model (LMM) for N pixels across P bands is formulated as:

$$\mathbf{Y} = \mathbf{E}\mathbf{A} + \mathbf{N} \quad \text{s.t.} \quad \mathbf{A} \geq 0,\ \mathbf{1}_R^\top \mathbf{A} = \mathbf{1}_N^\top \tag{1}$$

where $\mathbf{E} \in \mathbb{R}^{P\times R}$ contains R EMs, $\mathbf{A} \in \mathbb{R}^{R\times N}$ denotes fractional abundances, and $\mathbf{N}$ represents Gaussian noise. The LMM holds a strict geometric interpretation where noise-free pixels lie in an $(R-1)$ simplex that is spanned by the EMs.

2.2. Sparse and Redundant Models

Sparse and Redundant Models (SRMs) replace the unknown matrix $\mathbf{E}$ with a large known library $\mathbf{D} \in \mathbb{R}^{P \times M}$, solving:

$$\hat{\mathbf{X}} = \arg\min_{\mathbf{X}} \frac{1}{2}\|\mathbf{Y} - \mathbf{D}\mathbf{X}\|_F^2 + \lambda\|\mathbf{X}\|_1, \text{s.t. } \mathbf{X} \geq 0 \quad (2)$$

where $\mathbf{X}$ represents sparse abundances. Using the ℓ_1 norm for inducing sparsity is the most common choice for SRMs. Examples include the well-known Sparse Unmixing by Variable Splitting and Augmentend Lagrangian (**SUnSAL**) algorithm [3]. In [4], **MUA_SLIC**, a fast Multiscale Unmixing Algorithm was proposed, which uses simple linear iterative clustering segmentation to form uniform superpixels. It uses the superpixel information along with an ℓ_1 regularization. The authors in [5] propose a spectral-spatial weighted regression model (**S^{2}WSU**). It uses a doubly weighted sparsity framework based on both spectral and spatial info. A downside of the ℓ_1 penalty is that it is nondifferentiable at 0, complicating the optimization problems. Secondly, it is not compatible with the abundance sum-to-one constraint. This means that using the ℓ_1 penalty necessarily breaks the geometric interpretation of the linear mixing model.

Other sparsity penalties have also been proposed, such as the ℓ_2 norm [6]. This is known as collaborative sparsity (CL). **CLSUnSAL** is a variant of SUnSAL using CL. The ℓ_q norm with $0 \leq \ell \leq 1$ has also been used for unmixing [7]. Despite their efficacy, many sparse unmixing approaches often lack geometric and physical interpretations.

2.3. Archetypal Analysis Model

Library-based Archetypal Analysis Models (AAMs) assume that EMs are convex combinations of library entries [8]. Let $\mathbf{B}$ be a dictionary selection matrix, which is subject to a nonnegativity and sum-to-one constraint. Write the EMs as $\mathbf{E} = \mathbf{D}\mathbf{B}$. Then the AAM problem becomes:

$$\begin{aligned} &\mathbf{Y} = \mathbf{D}\mathbf{B}\mathbf{A} + \mathbf{N} \\ &\text{s.t. } \mathbf{B} \geq 0,\ \mathbf{1}_M^\top \mathbf{B} = \mathbf{1}_R^\top,\ \mathbf{A} \geq 0,\ \mathbf{1}_R^\top \mathbf{A} = \mathbf{1}_N^\top. \end{aligned} \quad (3)$$

One of the first AAM-based unmixing methods was Sparse Unmixing using Archetypal Analysis (**SUnAA**), which uses the sum-to-one constraint on the abundances and the dictionary selection matrix $\mathbf{B}$ [9]. It solves the problem using an active set algorithm. Fast Sparse Unmixing (**FaSUn**) uses a fast GPU-based ADMM approach to replace the slow active set optimization of SUnAA [10]. Sparse Unmixing using Soft Shrinkage (**SUnS**) modifies the core AAM formulation by substituting the sum-to-one constraint on $\mathbf{B}$ with an ℓ_1 sparsity regularizer, which is then solved using an ADMM-based approach [11].

AAMs preserve the geometric interpretation (abundance nonnegativity and sum-to-one constraints) and exhibit low-rank computational advantages but lead to nonconvex optimization problems, which are challenging to solve. Additionally, the number of EMs should be known, which makes it more challenging to solve compared to SRMs, which do not require this information.

3. PROPOSED METHOD: MISISUN

When pure pixels are absent from the image, AAM methods generate virtual EMs by combining library spectra. These generated virtual EMs might not correspond to the real EMs in the dataset, as there is no incentive in AAM for them to form realistic spectral signatures. To ensure physically meaningful virtual EMs, MiSiSUn imposes a center penalty

$$\lambda\|\mathbf{D}\mathbf{B} - \mathbf{m}\mathbf{1}_R^\top\|_F^2, \quad (4)$$

where $\mathbf{m} = \frac{1}{N}\mathbf{Y}\mathbf{1}_N$ is the mean of the data [12]. This term pulls estimated EMs inward and limits the simplex volume, closely aligning with the geometric interpretation of linear mixing models [2]. The resulting optimization problem optimizes over both $\mathbf{A}$ and $\mathbf{B}$:

$$\begin{aligned} &\min_{\mathbf{A},\mathbf{B}} \frac{1}{2}\|\mathbf{Y} - \mathbf{D}\mathbf{B}\mathbf{A}\|_F^2 + \lambda\|\mathbf{D}\mathbf{B} - \mathbf{m}\mathbf{1}_R^\top\|_F^2 \\ &\text{s.t. } \mathbf{B} \geq 0,\ \mathbf{1}_M^\top \mathbf{B} = \mathbf{1}_R^\top,\ \mathbf{A} \geq 0,\ \mathbf{1}_R^\top \mathbf{A} = \mathbf{1}_N^\top. \end{aligned} \quad (5)$$

We employ a block coordinate descent scheme to split the non-convex problem into two convex sub-steps solved via ADMM.

Abundance update – With $\mathbf{B}$ fixed, we define the EM matrix $\mathbf{E} = \mathbf{D}\mathbf{B}$. By introducing the splitting variable $\mathbf{S}$ and the Lagrange multiplier $\mathbf{L}$, we can write the Augmented Lagrangian

$$\begin{aligned} \mathcal{L}(\mathbf{A}, \mathbf{S}, \mathbf{L}) =& \frac{1}{2}\|\mathbf{Y} - \mathbf{E}\mathbf{A}\|_F^2 + \frac{\mu}{2}\|\mathbf{S} - \mathbf{A} - \mathbf{L}\|_F^2 \\ &\text{s.t. } \mathbf{S} \geq 0, \mathbf{1}_R^\top \mathbf{A} = \mathbf{1}_N^\top \end{aligned} \quad (6)$$

Solving via the Karush-Kuhn-Tucker (KKT) optimality conditions yields the closed-form update for $\mathbf{A}$:

$$\mathbf{A} \leftarrow (\mathbf{Q} + \mathbf{Q}\mathbf{1}_R c \mathbf{1}_R^\top \mathbf{Q})(\mathbf{E}^\top \mathbf{Y} + \mu(\mathbf{S} - \mathbf{L})) - \mathbf{Q}\mathbf{1}_R c \mathbf{1}_N^\top \quad (7)$$

with

$$\mathbf{Q} = (\mathbf{E}^\top \mathbf{E} + \mu \mathbf{I}_R)^{-1}$$

and

$$c = -1/(\mathbf{1}_R^\top \mathbf{Q} \mathbf{1}_R)$$

. This is followed by the split variable and multiplier update:

$$\mathbf{S} \leftarrow \max(0, \mathbf{A} + \mathbf{L}) \quad (8)$$

$$\mathbf{L} \leftarrow \mathbf{L} + \mathbf{A} - \mathbf{S}. \quad (9)$$

Dictionary selection update – With $\mathbf{A}$ fixed, we introduce split variables $\mathbf{B} = \mathbf{S}_1$ and $\mathbf{D}\mathbf{B} = \mathbf{S}_2$ and their corresponding Lagrange multipliers $\mathbf{L}_1$ and $\mathbf{L}_2$. Similarly to

the abundance update, we can formulate the augmented Lagrangian

$$\begin{aligned}\mathcal{L}_B(\mathbf{B},\mathbf{S}_1,\mathbf{S}_2,\mathbf{L}_1,\mathbf{L}_2) =& \frac{1}{2}\|\mathbf{Y}-\mathbf{S}_2\mathbf{A}\|_F^2+\lambda\|\mathbf{S}_2-\mathbf{m}\mathbf{1}_R^\top\|_F^2 \\ &+\frac{\mu_1}{2}\|\mathbf{S}_1-\mathbf{B}-\mathbf{L}_1\|_F^2+\frac{\mu_2}{2}\|\mathbf{S}_2-\mathbf{D}\mathbf{B}-\mathbf{L}_2\|_F^2, \\ &\text{s.t. } \mathbf{S}_2\geq 0, \mathbf{1}_M^\top\mathbf{B}=\mathbf{1}_R^\top\end{aligned} \tag{10}$$

We can again solve the KKT system to find the update rule for $\mathbf{B}$:

$$\begin{aligned}\mathbf{B}\leftarrow(\mathbf{Q}_\mathbf{B}+\mathbf{Q}_\mathbf{B}\mathbf{1}_M c_\mathbf{B}\mathbf{1}_M^\top\mathbf{Q}_\mathbf{B})\Big(\mathbf{D}^\top(\mathbf{S}_2-\mathbf{L}_2) \\ +\frac{\mu_1}{\mu_2}(\mathbf{S}_1-\mathbf{L}_1)\Big)-\mathbf{Q}_\mathbf{B}\mathbf{1}_M c_\mathbf{B}\mathbf{1}_R^\top\end{aligned} \tag{11}$$

where

$$\mathbf{Q}_\mathbf{B}=(\mathbf{D}^\top\mathbf{D}+\frac{\mu_1}{\mu_2}\mathbf{I}_M)^{-1}$$

and

$$c_\mathbf{B}=-1/(\mathbf{1}_M^\top\mathbf{Q}_\mathbf{B}\mathbf{1}_M).$$

The subsequent split variable and multiplier updates are:

$$\mathbf{S}_1\leftarrow\max(0,\mathbf{B}+\mathbf{L}_1) \tag{12}$$

$$\begin{aligned}\mathbf{S}_2\leftarrow(\mathbf{Y}\mathbf{A}^\top+\lambda\mathbf{m}\mathbf{1}_R^\top+\mu_2(\mathbf{D}\mathbf{B}+\mathbf{L}_2))(\mathbf{A}\mathbf{A}^\top \\ +(\mu_2+\lambda)\mathbf{I}_R)^{-1}\end{aligned} \tag{13}$$

$$\mathbf{L}_1\leftarrow\mathbf{L}_1+\mathbf{B}-\mathbf{S}_1 \tag{14}$$

$$\mathbf{L}_2\leftarrow\mathbf{L}_2+\mathbf{D}\mathbf{B}-\mathbf{S}_2 \tag{15}$$

We initialize all split variables and Lagrange multipliers with zero. Every block of update rules (the block for $\mathbf{A}$ and the block for $\mathbf{B}$) is repeated a fixed number of times, specified by the parameters T_A and T_B respectively. The overall algorithm terminates when this inner loop has run for a total of T times, where T is a user-defined parameter.

4. EXPERIMENTS

We compared the performance of MiSiSUn to eight semi-supervised unmixing methods, including four sparse regression models (SUnSAL [3], CLSUnSAL [13], MUA_SLIC [4] and S^{2}WSU [5]), three AAMs (SUnAA [9], SUnS [11] and FaSUn [10]) and one deep learning-based model, SUnCNN [14], which uses a convolutional neural network. For measuring the abundance estimation quality, we use the signal-to-reconstruction error (SRE) in dB:

$$\mathrm{SRE}(\mathbf{A},\widehat{\mathbf{A}})=10\log_{10}\frac{\|\mathbf{A}\|_F^2}{\|\mathbf{A}-\widehat{\mathbf{A}}\|_F^2}. \tag{16}$$

The hyperparameters for the different methods were fine-tuned to achieve the best possible performance. For the SRMs (SUnSAL, CLSUnSAL, MUA_SLIC, and S^{2}WSU), parameters were configured based on the SNR (more information can be found in the source code). Table 1 shows the fine-tuned hyperparameters for the two experiments.

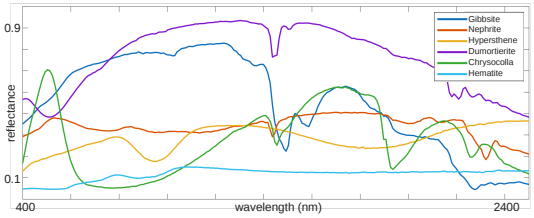


Fig. 1: EMs used in the simulated dataset

4.1. Simulated dataset

A simulated dataset of size 100×100 pixels was generated by linearly combining six EMs. These six EMs were obtained from the USGS Spectral Library, which contains 498 spectra. The EMs have a spectral range from 400 nm to 2,500 nm and 224 bands. The EMs are shown in Fig. 1. For abundance generation, we define a pixel purity parameter $\rho \leq 1$. An image with pixel purity parameter ρ has all abundance values less than or equal to ρ. Lower values therefore indicate a more highly mixed image. We sample the abundances from a symmetric Dirichlet distribution and discard all samples where a value exceeds ρ. In the end, we add Gaussian noise with an SNR of 30 dB. We performed hyperparameter tuning for all methods to achieve the best possible results. Afterwards, we performed five independent runs for each method and averaged the results. The resulting SREs are presented in Table 2. In general, the performance increases as the pixel purity level increases, which is to be expected. Archetypal analysis models significantly outperform sparse regression models, with the best performance being achieved by MiSiSUn in all cases, demonstrating the superior performance of the proposed approach, also in highly mixed scenarios. SUnAA and FaSUn achieve similar performance and are superior to that of SUnS.

4.2. Real dataset: Cuprite

We apply the methods to a 250 × 191 region of interest of the Cuprite dataset, which contains 188 bands (after removing noisy bands) from 370 to 2480 nm. We focus on the 5 dominant minerals (Alunite, Chalcedony, Kaolinite, Montmorillonite, and Sphene). The number of EMs in this scene was set to $R = 12$. As no ground truth is available, we perform a visual comparison to the geological reference map; see Fig. 2. AAMs produce physically meaningful abundance maps, with a visual inspection showing that MiSiSUn performs best, especially for Alunite and Chalcedony (first two rows in Fig. 2(b)). SRMs produce abundance maps with very low abundance values, since they distribute them over a large number of possible EMs, diluting the abundance maps for all EMs.

4.3. Computational efficiency

Table 3 shows the mean runtime of the different methods on the two datasets. As expected, processing times generally in-

Table 1: Hyperparameters used in the experiments for the Simulated and Cuprite datasets.

Methods	Simulated	Cuprite
SUnSAL	based on SNR	$\lambda = 0.005$
CLSUnSAL	based on SNR	$\lambda = 0.05$, $\mu = 0.01$
MUA_SLIC	based on SNR	$\lambda_1 = 0.001$, $\lambda_2 = 0.01$
S^2WSU	based on SNR	$\lambda = 0.001$
SUnCNN	based on SNR	iters $= 20000$
SUnAA	default	default
FaSUn	$T = 10000$, $T_A = T_B = 5$, $\mu_1 = 50$, $\mu_2 = 2$, $\mu_3 = 1$	$T = 10000$, $T_A = T_B = 5$, $\mu_1 = 400$, $\mu_2 = 20$, $\mu_3 = 1$
SUnS	$T = 10000$, $T_A = T_B = 5$, $\mu_1 = 50$, $\mu_2 = 2$, $\mu_3 = 1$	$T = 10000$, $T_A = T_B = 5$, $\mu_1 = 400$, $\mu_2 = 20$, $\mu_3 = 1$
MiSiSUn	$T = 10000$, $T_A = T_B = 5$, $\mu = 50$, $\mu_1 = 2$, $\mu_2 = 1$, $\lambda = 0.3$	$T = 10000$, $T_A = T_B = 5$, $\mu = 500$, $\mu_1 = 50$, $\mu_2 = 1$, $\lambda = 10$

Table 2: Average abundance SRE (in dB) for different pixel purities. The best results are highlighted in bold.

Algorithm	$\rho = 0.7$	$\rho = 0.85$	$\rho = 1.0$
SUnSAL	2.41	2.79	2.97
S2WSU	2.97	2.97	2.99
CLSUnSAL	4.07	5.86	7.23
MUA_SLIC	2.33	2.69	3.22
SUnCNN	12.83	13.96	7.38
SUnAA	21.79	23.98	23.18
FaSUn	22.46	22.88	23.50
SUnS	19.97	20.37	20.61
MiSiSUn (ours)	**24.23**	**25.83**	**26.08**

crease with image size. SUnSAL is the fastest method on both datasets. The sparse regression models (SRMs), i.e., the first four methods, exhibit a more pronounced increase in runtime as the number of pixels grows. In SRMs, the abundance matrix has dimensions $M \times N$, and dense variable updates may involve a computational complexity of $\mathcal{O}(NM^2)$. Although the factorization of the associated $M \times M$ system can typically be precomputed, the iterative updates remain dependent on both the dictionary size M and the number of pixels N.

In contrast, MiSiSUn, FaSUn, and SUnS estimate abundances in a reduced R-dimensional representation, where $R \ll M$, resulting in a pixel-dependent computational cost of $\mathcal{O}(NPR)$. Nevertheless, the dictionary-selection updates also depend on M. In particular, the $M \times M$ matrix inverse in the MiSiSUn B-update can be precomputed since the dictionary and penalty parameters remain fixed, while subsequent dense operations involve costs of $\mathcal{O}(M^2R)$ and $\mathcal{O}(PMR)$. Consequently, for $R \ll \min(P, M, N)$, the leading per-iteration computational cost is $\mathcal{O}(NPR + M^2R + PMR)$, excluding one-time preprocessing costs. This reduced dependence on the number of pixels and the use of a low-dimensional abundance representation contribute to the favorable scalability of these methods, particularly for large hyperspectral images.

5. CONCLUSION

This paper presented MiSiSUn, a novel library-based semisupervised hyperspectral unmixing method. By combining archetypal analysis models with a minimum simplex volume constraint, the algorithm generates highly authentic virtual endmembers for highly mixed scenarios. Experiments confirm its superior estimation accuracy and ability to generate physically realistic abundance maps. Additionally, due to its GPU implementation and linear computational complexity, MiSiSUn is scalable to large problem sizes.

In future work, we will investigate the extension of MiSiSUn to EM bundle-based approaches, which will further enhance its physical interpretability and estimation accuracy, and lower the computational cost.

Acknowledgement

The research presented in this paper is funded by the Research Foundation-Flanders (project G031921N). Xander Haijen is a PhD fellow of the Research Foundation Flanders, Belgium (FWO: 1103226N). The work of Bikram Koirala was supported by the Research Foundation Flanders, Belgium (FWO: 1250824N-7028). The authors thank Dr. Alexandre Zouaoui for providing the codes for competing methods.

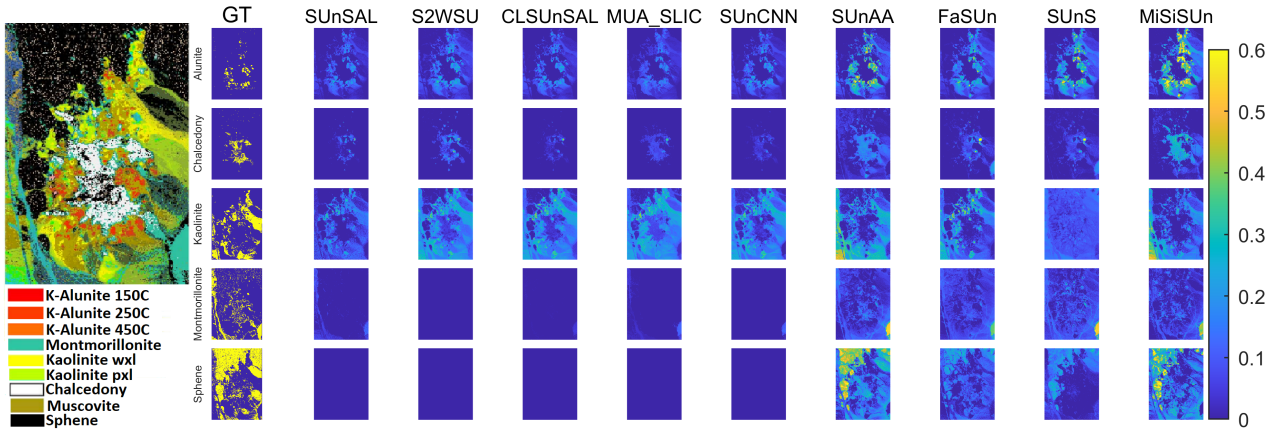
6. REFERENCES

[1] B. Rasti, A. Zouaoui, J. Mairal, and J. Chanussot, "Image processing and machine learning for hyperspectral unmixing: An overview and the hysupp python package," *arXiv*, 2023.

[2] J.M. Bioucas-Dias, A. Plaza, N. Dobigeon, M. Parente, Qian Du, P. Gader, and J. Chanussot, "Hyperspectral unmixing overview: Geometrical, statistical, and sparse regression-based approaches," *IEEE J. Sel. Topics Appl. Earth Observ. Remote Sens.*, vol. 5, no. 2, pp. 354–379, April 2012.

Table 3: Processing time for the considered methods on the two datasets. The best results are highlighted in bold.

	N	P	R	M	SUnSAL	S2WSU	CLSUnSAL	MUA_SLIC	SUnCNN	SUnAA	FaSUn	SUnS	MiSiSUn
Simulated	10000	224	6	498	**20.5**	84.7	56.9	38.9	60.0	159.0	111.3	115.3	113.2
Cuprite	47750	188	12	498	**47.7**	321.4	175.6	116.9	565.8	195.5	134.4	134.0	138.7



(a) Reference Map

(b) Estimated abundances

Fig. 2: Abundance maps obtained by the different methods on Cuprite, along with the geological reference map and the produced GT abundance maps from this reference.

[3] J.M. Bioucas-Dias and M. A T Figueiredo, "Alternating direction algorithms for constrained sparse regression: Application to hyperspectral unmixing," in *2nd Workshop on Hyperspectral Image and Signal Processing: Evolution in Remote Sensing (WHISPERS), 2010*, 2010, pp. 1–4.

[4] R. A. Borsoi, T. Imbiriba, J. C. M. Bermudez, and C. Richard, "A fast multiscale spatial regularization for sparse hyperspectral unmixing," *IEEE Geosci. Remote Sens. Lett.*, vol. 16, no. 4, pp. 598–602, 2019.

[5] S. Zhang, J. Li, H. Li, C. Deng, and A. Plaza, "Spectral–spatial weighted sparse regression for hyperspectral image unmixing," *IEEE Trans. Geosci. Remote Sens.*, vol. 56, no. 6, pp. 3265–3276, 2018.

[6] M. Iordache, J. M. Bioucas-Dias, and A. Plaza, "Collaborative sparse regression for hyperspectral unmixing," *IEEE Trans. Geosci. Remote Sens.*, vol. 52, no. 1, pp. 341–354, Jan 2014.

[7] J. Sigurdsson, M.O. Ulfarsson, and J.R. Sveinsson, "Hyperspectral unmixing with l_q regularization," *IEEE Trans. Geosci. Remote Sens.*, vol. 52, no. 11, pp. 6793–6806, 2014.

[8] A. Zouaoui, G. Muhawenayo, B. Rasti, J. Chanussot, and J. Mairal, "Entropic descent archetypal analysis for blind hyperspectral unmixing," *IEEE Trans. Image Process.*, pp. 1–1, 2023.

[9] B. Rasti, A. Zouaoui, J. Mairal, and J. Chanussot, "Sunaa: Sparse unmixing using archetypal analysis," *IEEE Geosci. Remote Sens. Lett.*, pp. 1–1, 2023.

[10] B. Rasti, "Fasun: Fast semi-supervised unmixing using alternating direction method of multipliers," in *13th Workshop on Hyperspectral Imaging and Signal Processing: Evolution in Remote Sensing (WHISPERS)*, 2023, pp. 1–5.

[11] B. Rasti, A. Zouaoui, J. Mairal, and J. Chanussot, "Fast semi-supervised unmixing using non-convex optimization," 2024.

[12] L. Zhuang, C. Lin, M. A. T. Figueiredo, and J. M. Bioucas-Dias, "Regularization parameter selection in minimum volume hyperspectral unmixing," *IEEE Trans. Geosci. Remote Sens.*, vol. 57, no. 12, pp. 9858–9877, 2019.

[13] M. D. Iordache, J. M. Bioucas-Dias, and A. Plaza, "Total variation spatial regularization for sparse hyperspectral unmixing.," *IEEE Trans. Geosci. Remote Sens.*, vol. 50, no. 11, pp. 4484–4502, Nov 2012.

[14] B. Rasti and B. Koirala, "SUnCNN: Sparse unmixing using unsupervised convolutional neural network," *IEEE Geosci. Remote Sens. Lett.*, vol. 19, pp. 1–5, 2022.